

Radiative corrections to stoponium annihilation decays

Stephen P. Martin^{1,2} and James E. Younkin¹

¹*Department of Physics, Northern Illinois University, DeKalb IL 60115 and*

²*Fermi National Accelerator Laboratory, P.O. Box 500, Batavia IL 60510*

The lighter top squark in supersymmetry can live long enough to form hadronic bound states if it has no kinematically allowed two-body decays that conserve flavor. In this case, scalar stoponium may be observable through its diphoton decay mode at the CERN Large Hadron Collider, enabling a uniquely precise measurement of the top-squark mass. The viability of the signal depends crucially on the branching ratio to diphotons. We compute the next-to-leading order QCD radiative corrections to stoponium annihilation decays to hadrons, photons, and Higgs scalar bosons. We find that the effect of these corrections is to significantly decrease the predicted branching ratio to the important diphoton channel. We also find a greatly improved renormalization-scale dependence of the diphoton branching ratio prediction.

Contents

I. Introduction	2
II. Decays to hadrons and to photons	4
III. Decays to Higgs scalar bosons	12
IV. Numerical results	15
V. Outlook	17
References	19

I. INTRODUCTION

The Minimal Supersymmetric Standard Model (MSSM) [1] with conserved R-parity contains a stable lightest supersymmetric particle (LSP). If the LSP is neutral, it could be the cold dark matter required by the standard cosmology. The collider signatures of the MSSM generally involve missing energy carried away by two LSPs produced in each event. Unfortunately, this suggests that there will be no true kinematic mass peaks whose reconstruction would determine superpartner masses. In favorable models, it is possible to obtain precision measurements of superpartner mass differences and other combinations of masses at hadron colliders by finding kinematic edges from decays. However, the overall mass scale of the superpartners will be much harder to obtain precisely at the CERN Large Hadron Collider [2, 3].

In models with a relatively small mass difference between the lighter top squark \tilde{t}_1 and the neutralino LSP \tilde{N}_1 , there is an exception that would allow a sharp mass peak. If the lighter top squark has no kinematically allowed two-body decays that conserve flavor, then it will form hadronic bound states. Among these is stoponium, a stop-anti-stop bound state, which can be directly produced at hadron colliders through gluon-gluon fusion. The largest production cross-section is for the $1S$ ($J^{PC} = 0^{++}$) state, denoted in the following by $\eta_{\tilde{t}}$, but other stoponium states can contribute to the signal either by prompt decays to the ground state or direct annihilation decays. This state will form if

$$m_{\tilde{t}_1} < m_{\tilde{N}_1} + m_t, \quad (1.1)$$

$$m_{\tilde{t}_1} < m_{\tilde{C}_1} + 5 \text{ GeV}, \quad (1.2)$$

so that the decays $\tilde{t}_1 \rightarrow t\tilde{N}_1$ and $\tilde{t}_1 \rightarrow b\tilde{C}_1$ are both kinematically forbidden. (Here \tilde{C}_1 stands for the lighter chargino mass eigenstate.) These conditions are almost never satisfied in the MSSM parameter space with the so-called mSUGRA boundary conditions, but they can easily be satisfied in other motivated models. These include “compressed supersymmetry” models [4] in which the predicted thermal relic density of dark matter is in agreement with that observed by WMAP and other experiments [5]-[7], due to the enhanced annihilation $\tilde{N}_1\tilde{N}_1 \rightarrow t\bar{t}$ mediated by t -channel exchange of top squarks.[†] Another class of models consists of those that generate the baryon excess over anti-baryons at the electroweak scale [11], [9], [12]. In these and other [13] cases, $m_{\tilde{t}_1} - m_{\tilde{N}_1}$ is necessarily small enough to guarantee the formation of stoponium.

Stoponium can decay directly by the decays of one of the top-squark constituents through the 3-body process $\tilde{t}_1 \rightarrow Wb\tilde{N}_1$, or if that is kinematically forbidden, through the flavor-violating 2-body process $\tilde{t}_1 \rightarrow c\tilde{N}_1$ and/or the 4-body process $\tilde{t}_1 \rightarrow f\bar{f}'b\tilde{N}_1$. However, the corresponding partial widths are many orders of magnitude smaller [14]-[18] than the binding energy of stoponium, which will be of order a few GeV [19]. Therefore, $\eta_{\tilde{t}}$ will decay primarily by annihilation, including the possible two-body final states gg , $\gamma\gamma$, h^0h^0 , W^+W^- , ZZ , $Z\gamma$, $t\bar{t}$, and $b\bar{b}$. Of these, the most promising final state, both for detectability over backgrounds and reconstruction of the mass peak, is $\gamma\gamma$, as was first pointed out long ago by Drees and Nojiri [20, 21] (See also refs. [22]-[28] for other work related to stoponium at colliders.) The diphoton stoponium signals for both compressed

[†] The inequalities (1.1) and (1.2) can also be satisfied in the stop-neutralino co-annihilation region [8]-[10] of parameter space, but at the price of a much more extreme fine-tuning of input parameters.

supersymmetry and supersymmetric electroweak-scale baryogenesis have recently been studied in [29].

In much of the parameter space in which stoponium can form, the gg two-body final state leading to hadronic jets dominates. If so, then the leading-order prediction for $\text{BR}(\gamma\gamma)$ is nearly model-independent, and is of order 0.005. The QCD corrections to the bound state annihilation decays are quite significant, however, and need to be taken into account along with corrections to the production cross-section in order to obtain a realistic estimate of the LHC sensitivity for a given model. In this paper, we will calculate the QCD next-to-leading order corrections to S -wave stoponium[‡] decay into the $\gamma\gamma$, gg , and h^0h^0 final states. The decay widths into $\gamma\gamma$ and gg are model-independent to leading order, and one may also argue that they are the most important, since gg usually dominates the total width, and $\gamma\gamma$ is the observable signal. However, the h^0h^0 final state may dominate in some parts of parameter space, particularly if stoponium is just above the threshold for that decay.

We will proceed following the strategy (and some of the notation) used in ref. [30] where the analogous case of quarkonium decay was studied. (The quarkonium annihilation beyond leading order was calculated earlier in ref. [31], which regulated infrared divergences and mass singularities using a gluon mass instead of dimensional regularization.) The S -wave stoponium decay width is related to the low-velocity ($v \rightarrow 0$) limit of the stop-anti-stop annihilation cross-section by:

$$\Gamma(\eta_{\tilde{t}} \rightarrow X) = v\sigma(\tilde{t}_1\tilde{t}_1^* \rightarrow X)|\Psi(0)|^2, \quad (1.3)$$

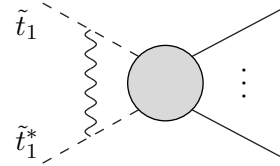
where $\Psi(0)$ is the bound-state wavefunction at the origin. [This is often expressed instead in terms of the radial wavefunction at the origin, $R(0) = \sqrt{4\pi}\Psi(0)$.] Here, v is the relative velocity of the squarks in the center-of-momentum frame. (The same formula (1.3) holds for excited states with 0 angular momentum. Obtaining the decay widths of higher angular momentum stoponium states would require keeping contributions at higher order in v .) For diphoton and hadronic final states, the cross-section on the right-hand side of eq. (1.3) is in turn related by the optical theorem to the imaginary part of the amplitude for $\tilde{t}_1\tilde{t}_1^* \rightarrow \tilde{t}_1\tilde{t}_1^*$ through two-particle and three-particle cuts. For the h^0h^0 final state, we find it easier to just calculate the radiative corrections to the decay directly. In both cases, we work in Feynman gauge, and regulate amplitudes using dimensional regularization in $d = 4 - 2\epsilon$ dimensions. Ultraviolet divergences are indicated separately by writing $1/\epsilon_{\text{UV}}$, while infrared divergences and mass singularities are indicated by $1/\epsilon_{\text{IR}}$ and $1/\epsilon_{\text{IR}}^2$ for the pole terms. The top-squark propagator is renormalized on-shell, and the QCD gauge coupling will be renormalized in the $\overline{\text{MS}}$ scheme.

An important issue that arises in all calculations of this type is that $\sigma(\tilde{t}_1\tilde{t}_1^* \rightarrow X)$ obtains contributions that are divergent as $v \rightarrow 0$ due to the exchange of massless gluons in diagrams of the form shown in figure 1. The relevant next-to-leading order contribution in QCD is related to the leading order contribution by

$$\Delta\sigma^{(1)}(\tilde{t}_1\tilde{t}_1^* \rightarrow X) = \left[\frac{\pi\alpha_S}{v} C_F + \mathcal{O}(v^0) \right] \sigma^{(0)}(\tilde{t}_1\tilde{t}_1^* \rightarrow X), \quad (1.4)$$

[‡] Although we have in mind the top squark, our results can also be applied to any new strongly interacting fundamental scalar whose width is small enough that it hadronizes before it decays.

FIG. 1: Diagrams contributing to $\tilde{t}_1\tilde{t}_1^* \rightarrow X$ with gluon exchange between the initial state squarks, leading to Coulomb $1/v$ singularities of the type in eq. (1.4).



where C_F is the quadratic Casimir invariant, $4/3$ for $SU(3)$. This Coulomb singularity can be absorbed into the definition of the bound state wave-function $\Psi(0)$. Alternatively, since it is universal in character, it cancels when one considers branching ratio observables. This provides a useful test of the calculation.

The rest of this paper is organized as follows. In section II, we find the next-to-leading order QCD corrections to stoponium annihilations into gg and $\gamma\gamma$ final states. Section III discusses the one-loop QCD corrections for the h^0h^0 final state. In section IV, we discuss the numerical impact of these results. Section V contains some concluding remarks.

II. DECAYS TO HADRONS AND TO PHOTONS

In this section, we calculate the next-to-leading order QCD corrections to the gg and $\gamma\gamma$ partial widths. We use the cut method derived from the optical theorem, which allows the direct computation of the squared amplitude and avoids having to square a matrix element involving many terms. To calculate the amplitude for an arbitrary process $X \rightarrow Y$, draw all of the diagrams involving $X \rightarrow X$ scattering to the desired order, then cut the diagrams through the propagators that correspond to the desired final state Y (for $\tilde{t}\tilde{t}^* \rightarrow gg$ at leading order, we have the three diagrams in figure 3). These cut propagators are put on mass-shell, using the appropriate Feynman rule corresponding to external particles (see Figure 2). Then the sum of all cut diagrams, multiplied by an extra factor of -1 and summed and averaged over spins and colors as appropriate, is denoted by \mathcal{M}_{cut} and equals the squared amplitude of $X \rightarrow Y$.

In order to get the partial widths, the contributions to \mathcal{M}_{cut} must be integrated over d -dimensional Lorentz-invariant phase space. The individual contribution of a single cut diagram to the cross-section is

$$\begin{aligned} \Delta\sigma &= \frac{1}{4E_A E_B v} \int \mathcal{M}_{\text{cut}} \left(\prod_f \mu^{2\epsilon} \frac{d^d k_f}{(2\pi)^{d-1}} \delta(k_f^2 - m_f^2) \theta(k_f^0) \right) (2\pi)^d \delta^{(d)}(p_A + p_B - \sum_f k_f) \\ &\equiv \frac{1}{4E_A E_B v} \int \mathcal{M}_{\text{cut}} \text{dLIPS}_N. \end{aligned} \quad (2.1)$$

In equation (2.1), the labels A and B are for the initial-state and f for the final-state momentum four-vectors, v is the relative velocity of the initial-state particles, and $\int \text{dLIPS}_N$ is the integral over N -body Lorentz-invariant phase space. Since we are calculating the annihilation of a bound state, we multiply both sides by the relative velocity and set $E_A = E_B = m_{\tilde{t}_1}$ as the relative velocity goes to zero. Therefore,

$$v\Delta\sigma = \frac{1}{4m_{\tilde{t}_1}^2} \int \mathcal{M}_{\text{cut}} \text{dLIPS}_N. \quad (2.2)$$

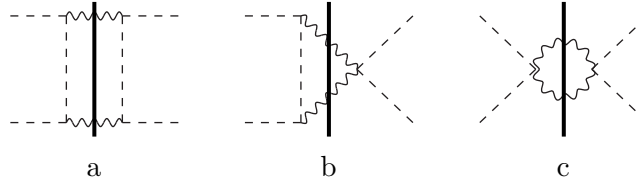


FIG. 3: The diagrams whose imaginary parts contribute to the annihilation of $\tilde{t}_1\tilde{t}_1^*$ into gauge bosons at leading order. The dark bars indicate where the diagrams have been cut. Diagrams related by permutations of external lines and arrow-reversal are not distinguished.

gg result. For this final state,

$$v\sigma^{(0)}(\tilde{t}_1\tilde{t}_1^* \rightarrow \gamma\gamma) = \frac{2N_c\pi Q_s^4\alpha^2}{m_{\tilde{t}_1}^2} \frac{\Gamma(2-\epsilon)}{\Gamma(2-2\epsilon)} \left(\frac{\pi\mu^4}{m_{\tilde{t}_1}^2}\right)^\epsilon, \quad (2.4)$$

where $Q_s = +2/3$ is the charge of the squark, and $\alpha = e^2/4\pi$. Therefore, the leading-order decay rates are

$$\Gamma^{(0)}(\eta_{\tilde{t}} \rightarrow gg) = \frac{16\pi}{3}\alpha_S^2 \frac{|\Psi(0)|^2}{m_{\eta_{\tilde{t}}}^2}, \quad (2.5)$$

$$\Gamma^{(0)}(\eta_{\tilde{t}} \rightarrow \gamma\gamma) = \frac{128\pi}{27}\alpha^2 \frac{|\Psi(0)|^2}{m_{\eta_{\tilde{t}}}^2}, \quad (2.6)$$

where we have replaced the bare coupling $\hat{\alpha}_S$ with the renormalized coupling α_S , since they are equal at leading order. Taking the ratio of these partial widths eliminates the bound state wavefunction and produces the simple leading-order result

$$R^{(0)} \equiv \frac{\Gamma^{(0)}(\eta_{\tilde{t}} \rightarrow \gamma\gamma)}{\Gamma^{(0)}(\eta_{\tilde{t}} \rightarrow gg)} = \frac{8\alpha^2}{9\alpha_S^2}. \quad (2.7)$$

The non-vanishing cut diagrams that correspond to the annihilation of $\tilde{t}_1\tilde{t}_1^*$ into gg , ggg , and $gq\bar{q}$ final states at next-to-leading order are given in figure 4[†]. Many of these diagrams can be cut in more than one way. In diagrams with three cut propagators, there is either real gluon emission or the pair-production of quarks[‡], and diagrams with two cut propagators have one-loop integrals.

In diagrams with three-particle cuts, the principal difficulty is integrating the momentum fractions of the final-state particles over three-body phase space. To do this, the phase space integrals can be reduced to integrals of the form given in the Appendix of ref. [30]. Care must be taken in

[†] Note that several diagrams not shown in the figure vanish because the color indices of three-gluon final states must be antisymmetric by charge conjugation invariance. This is because $\eta_{\tilde{t}}$ has $C = +1$, while a final state with n gluons has $C = (-1)^{n+n_c}$, where n_c is 1 (0) for antisymmetric (symmetric) adjoint color indices [32].

[‡] We include some $gq\bar{q}$ final state contributions, even though these may be regarded as corrections to $q\bar{q}$ final states, which we do not treat here. The light $q\bar{q}$ partial widths are suppressed by small Yukawa couplings at leading order, and the $t\bar{t}$ final state is often strongly suppressed by kinematics and couplings. However, the $gq\bar{q}$ contributions from 3-particle cuts in diagrams p1, p2, and p3 in figure 4 cancel large logarithms in the limit of small m_q due to the gluon vacuum polarization (2-particle cut) contributions from the same diagrams.

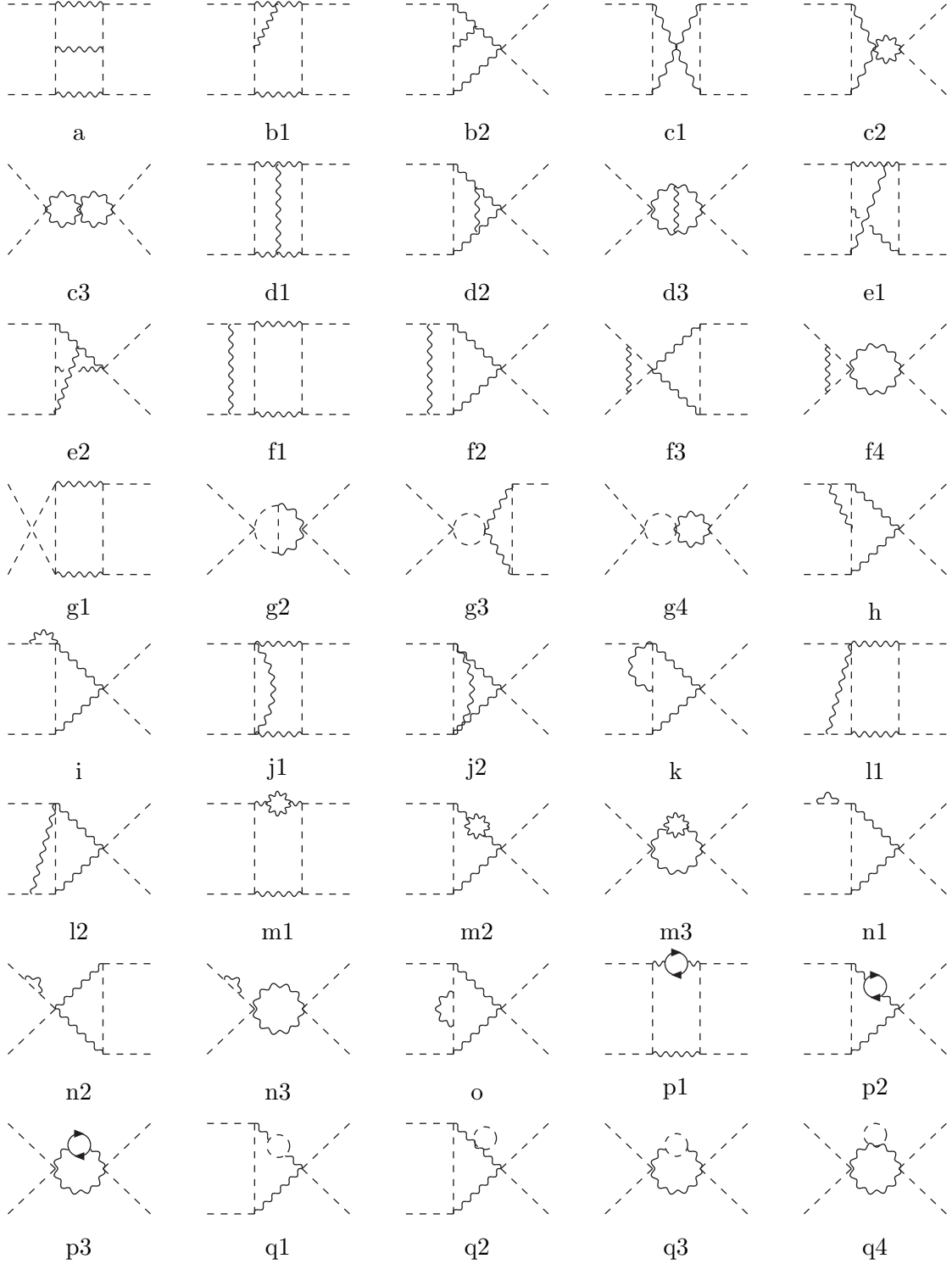


FIG. 4: The diagrams whose imaginary parts contribute to the cross-section for $\tilde{t}_1 \tilde{t}_1^* \rightarrow gg$ at next-to-leading order, including ggg and $gq\bar{q}$. Each diagram must be cut in all the ways it is possible to put the cut propagators simultaneously on-shell, and the propagators that are cut indicate the corresponding two- or three-particle final state. Diagrams related by permutations of external states and arrow-reversal are not shown, nor are the diagrams with ghost loops that are needed for each diagram with a gauge boson loop. We have also not shown several diagrams that vanish for all possible cuts.

evaluating diagrams with multiple distinct three-propagator cuts. Diagram d2, for example, has two cuts that are not equal.

Evaluation of the two-particle cuts involves expanding the loop integral from the virtual gluon in partial fractions to obtain a set of scalar integrals, which are well-known. A complete set of scalar integrals that occur in the calculation can be found in ref. [33] (for a complete set of divergent and many finite scalar loop integrals, see ref. [34]). In contrast with the three-particle cuts, the phase space integration is quite easy [30]. Since the cut diagrams do not depend on the final-state momentum directions, they are proportional to their contributions to the cross-section

$$v\Delta\sigma^{(1)} = \frac{1}{4m_{\tilde{t}_1}^2} \mathcal{M}_{\text{cut}} \Phi(2), \quad (2.8)$$

where

$$\Phi(2) \equiv \int d\text{LIPS}_2 = \frac{1}{8\pi} \left(\frac{\pi}{m_{\tilde{t}_1}^2} \right)^\epsilon \frac{\Gamma(1-\epsilon)}{\Gamma(2-2\epsilon)}. \quad (2.9)$$

There is an important simplification that can be made in the massless two-particle cuts of diagrams with potential Coulomb singularities (diagrams f1, f2, f3, and f4 in figure 4). Using the identities [30]

$$\int d\text{LIPS}(P = k_1 + k_2) k_1^\mu = \frac{1}{2} P^\mu \Phi(2) \quad (2.10)$$

$$\int d\text{LIPS}(P = k_1 + k_2) k_1^\mu k_1^\nu = \frac{1}{4} \left(\frac{d}{d-1} P^\mu P^\nu - \frac{1}{d-1} P^2 g^{\mu\nu} \right) \Phi(2), \quad (2.11)$$

where k_1 and k_2 are the final-state gluon momentum 4-vectors, $d \equiv 4-2\epsilon$ is the number of spacetime dimensions, and $\Phi(2)$ the integrated two-body phase space, it is easy to show that, for integrals performed in this calculation, dot products of the particle momentum 4-vectors in the numerators of loop integrals cannot contain terms linear in the relative velocity v . The effect of the $v \rightarrow 0$ divergence comes only from the scalar loop integrals in the calculation, and one may set $v = 0$ everywhere else.

In Tables I and II, the contribution C_{diagram} from each diagram to $v\sigma^{(1)}(\tilde{t}_1\tilde{t}_1^* \rightarrow gg)$ is given in the form

$$v\Delta\sigma^{(1)}(\tilde{t}_1\tilde{t}_1^* \rightarrow gg) = v\sigma^{(0)}(\tilde{t}_1\tilde{t}_1^* \rightarrow gg) \frac{\hat{\alpha}_S}{\pi} f(\epsilon) C_{\text{diagram}}. \quad (2.12)$$

Here,

$$f(\epsilon) = \left(\frac{\pi\mu^2}{m_{\tilde{t}_1}^2} \right)^\epsilon \Gamma(1+\epsilon), \quad (2.13)$$

in keeping with the notation of ref. [30]. Also, C_F is the quadratic Casimir invariant, C_A is the Casimir invariant of the adjoint representation, and T_F is the index of the fundamental represen-

diagram	$C_{\text{diagram, three particle cut}}$	$C_{\text{diagram, two particle cut}}$
a	$C_A \left(\frac{5}{2} - \frac{\pi^2}{4} \right)$	0
b1	$C_A \left(\frac{5}{2} - \frac{\pi^2}{3} \right)$	0
b2	$C_A \left(-\frac{1}{8\epsilon_{\text{IR}}^2} - \frac{5}{8\epsilon_{\text{IR}}} - \frac{17}{8} + \frac{\pi^2}{12} \right)$	$C_A \left(\frac{1}{8\epsilon_{\text{IR}}^2} + \frac{5}{8\epsilon_{\text{IR}}} - \frac{3}{8\epsilon_{\text{UV}}} + \frac{1}{4} \ln(2) + \frac{1}{2} - \frac{\pi^2}{48} \right)$
c1	0	$C_A \left(-\frac{3}{16\epsilon_{\text{UV}}} - \frac{25}{48} - \frac{1}{24} \ln(2) \right)$
c2	0	$C_A \left(\frac{3}{2\epsilon_{\text{UV}}} + \frac{7}{2} \right)$
c3	0	$C_A \left(-\frac{3}{\epsilon_{\text{UV}}} - \frac{11}{2} \right)$
d1	$C_A \left(\frac{1}{2\epsilon_{\text{IR}}^2} + \frac{1}{\epsilon_{\text{IR}}} - \frac{\pi^2}{6} \right)$	$C_A \left(-\frac{1}{2\epsilon_{\text{IR}}^2} - \frac{1}{\epsilon_{\text{IR}}} + \frac{3}{16\epsilon_{\text{UV}}} - \frac{71}{48} + \frac{\pi^2}{3} + \frac{13}{24} \ln(2) \right)$
d2	$C_A \left(-\frac{7}{4\epsilon_{\text{IR}}^2} - \frac{3}{\epsilon_{\text{IR}}} - \frac{23}{4} + \frac{7\pi^2}{6} \right)$	$C_A \left(\frac{7}{4\epsilon_{\text{IR}}^2} + \frac{3}{\epsilon_{\text{IR}}} - \frac{15}{8\epsilon_{\text{UV}}} + \frac{11}{8} - \frac{7\pi^2}{6} - 2 \ln(2) \right)$
d3	$C_A \left(\frac{9}{4\epsilon_{\text{IR}}^2} + \frac{3}{\epsilon_{\text{IR}}} + \frac{33}{4} - \frac{3\pi^2}{2} \right)$	$C_A \left(-\frac{9}{4\epsilon_{\text{IR}}^2} - \frac{3}{\epsilon_{\text{IR}}} + \frac{9}{2\epsilon_{\text{UV}}} + \frac{9}{2} + \frac{3\pi^2}{2} \right)$
e1	0	$C_A \left(1 - \frac{\pi^2}{16} + \frac{1}{2} \ln(2) \right)$
e2	$C_A \left(\frac{1}{8\epsilon_{\text{IR}}^2} + \frac{5}{8\epsilon_{\text{IR}}} + \frac{17}{8} + \frac{\pi^2}{24} \right)$	$C_A \left(-\frac{1}{8\epsilon_{\text{IR}}^2} - \frac{5}{8\epsilon_{\text{IR}}} - \frac{21}{8} - \frac{11\pi^2}{48} + \frac{5}{4} \ln(2) \right)$
f1	0	$C_F \left(\frac{1}{4\epsilon_{\text{UV}}} - \frac{1}{4} + \frac{5\pi^2}{16} - \frac{3}{2} \ln(2) \right)$
f2	0	$C_F \left(-\frac{1}{2\epsilon_{\text{IR}}} - \frac{1}{\epsilon_{\text{UV}}} - \frac{\pi^2}{2v} - \frac{3}{2} - \frac{3\pi^2}{16} - 4 \ln(2) \right)$
f3	0	$C_F \left(-\frac{1}{2\epsilon_{\text{IR}}} - \frac{1}{4\epsilon_{\text{UV}}} - \frac{\pi^2}{2v} - \frac{1}{4} - \frac{3}{2} \ln(2) \right)$
f4	0	$C_F \left(\frac{2}{\epsilon_{\text{IR}}} + \frac{1}{\epsilon_{\text{UV}}} + \frac{2\pi^2}{v} - \frac{1}{2} + 6 \ln(2) \right)$
g1	0	$C_F \left(-\frac{1}{4\epsilon_{\text{UV}}} + \frac{1}{4} - \frac{\pi^2}{16} - \frac{1}{2} \ln(2) \right)$
g2	0	$C_F \left(\frac{1}{\epsilon_{\text{UV}}} + 2 - \frac{\pi^2}{16} + 2 \ln(2) \right)$
g3	0	$C_F \left(\frac{1}{4\epsilon_{\text{UV}}} + \frac{3}{4} + \frac{1}{2} \ln(2) \right)$
g4	0	$C_F \left(-\frac{1}{\epsilon_{\text{UV}}} - \frac{5}{2} - 2 \ln(2) \right)$
h	0	$(C_F - \frac{1}{2}C_A) \left(-\frac{1}{2\epsilon_{\text{UV}}} - \frac{3}{2} \right)$
i	0	$(C_F - \frac{1}{4}C_A) \left(\frac{3}{4\epsilon_{\text{UV}}} + \frac{3}{2} \ln(2) + \frac{5}{2} \right)$
j1	0	$(C_F - \frac{1}{4}C_A) \left(\frac{1}{\epsilon_{\text{UV}}} + 3 \right)$
j2	0	$(C_F - \frac{1}{4}C_A) \left(-\frac{4}{\epsilon_{\text{UV}}} - 10 \right)$
k	0	$(C_F - \frac{1}{4}C_A) \left(\frac{3}{4\epsilon_{\text{UV}}} + 2 + \frac{1}{2} \ln(2) \right)$
l1	0	$(C_F - \frac{1}{4}C_A) \left(-\frac{1}{2\epsilon_{\text{UV}}} - \frac{7}{2} + \frac{\pi^2}{8} + \ln(2) \right)$
l2	0	$(C_F - \frac{1}{4}C_A) \left(\frac{2}{\epsilon_{\text{UV}}} + 8 - \frac{3\pi^2}{8} - \ln(2) \right)$

TABLE I: Results for diagrams not involving propagator corrections to the tree level diagrams.

tation, given for $SU(3)$ by $C_F = 4/3$, $C_A = 3$, and $T_F = 1/2$. We have combined diagrams $q1$ with $q2$ and $q3$ with $q4$ in the table because the individual self-energy diagrams are not proportional to the projector $g^{\mu\nu} - q^\mu q^\nu / q^2$.

diagram	$C_{\text{diagram, three particle cut}}$	$C_{\text{diagram, two particle cut}}$
m1	$C_A \left(-\frac{5}{12\epsilon_{\text{IR}}} - \frac{61}{36} \right)$	0
m2	0	$C_A \left(\frac{5}{6\epsilon_{\text{IR}}} - \frac{5}{6\epsilon_{\text{UV}}} \right)$
m3	$C_A \left(\frac{5}{4\epsilon_{\text{IR}}} + \frac{17}{4} \right)$	$C_A \left(\frac{5}{3\epsilon_{\text{UV}}} - \frac{5}{3\epsilon_{\text{IR}}} \right)$
n1	0	$C_F \left(\frac{1}{2\epsilon_{\text{IR}}} - \frac{1}{2\epsilon_{\text{UV}}} \right)$
n2	0	$C_F \left(\frac{1}{2\epsilon_{\text{IR}}} - \frac{1}{2\epsilon_{\text{UV}}} \right)$
n3	0	$C_F \left(\frac{2}{\epsilon_{\text{UV}}} - \frac{2}{\epsilon_{\text{IR}}} \right)$
o	0	$C_F \left(-\frac{1}{2\epsilon_{\text{UV}}} - \frac{3}{2} - \ln(2) \right)$
p1	$\sum_f T_F \left(\frac{8}{9} + \frac{1}{3} \ln(m_f^2/4m_{\tilde{t}_1}^2) + h(m_f^2/m_{\tilde{t}_1}^2) \right)$	0
p2	0	$\sum_f T_F \left(\frac{2}{3\epsilon_{\text{UV}}} + \frac{2}{3} - \frac{2}{3} \ln(m_f^2/4m_{\tilde{t}_1}^2) \right)$
p3	$\sum_f T_F \left(-\frac{8}{3} - \ln(m_f^2/4m_{\tilde{t}_1}^2) - 3h(m_f^2/m_{\tilde{t}_1}^2) \right)$	$\sum_f T_F \left(-\frac{4}{3\epsilon_{\text{UV}}} - \frac{2}{3} + \frac{4}{3} \ln(m_f^2/4m_{\tilde{t}_1}^2) \right)$
q1 + q2	0	$T_F \left(\frac{1}{6\epsilon_{\text{UV}}} + \frac{1}{6} + \frac{1}{3} \ln(2) \right)$
q3 + q4	0	$T_F \left(-\frac{1}{3\epsilon_{\text{UV}}} - \frac{1}{6} - \frac{2}{3} \ln(2) \right)$

TABLE II: Results for diagrams involving propagator corrections to the tree-level diagrams. The function $h(m_f^2/m_{\tilde{t}_1}^2)$ is defined in eq. (2.16).

Taking the sum of the diagrams, we find the next-to-leading order result

$$\begin{aligned}
v\sigma^{(1)}(\tilde{t}_1\tilde{t}_1^* \rightarrow gg) &= v\sigma^{(0)}(\tilde{t}_1\tilde{t}_1^* \rightarrow gg) \left\{ 1 + f(\epsilon) \frac{\hat{\alpha}_S}{\pi} \left[\frac{b_0}{2\epsilon_{\text{UV}}} + \left(\frac{199}{18} - \frac{13\pi^2}{24} \right) C_A \right. \right. \\
&\quad + \left(\frac{\pi^2}{v} - \frac{7}{2} - \frac{\pi^2}{8} + \left(\frac{1}{2} - \frac{\pi^2}{8} \right) \delta \right) C_F \\
&\quad \left. \left. + \left(-\frac{16}{9}(n_{\text{light}} + n_t) - 2n_t h(m_t^2/m_{\tilde{t}_1}^2) - \frac{1}{3} \ln(2) \right) T_F \right] \right\}, \quad (2.14)
\end{aligned}$$

where δ is either 1 or 0 depending on whether or not the four-point squark interaction in Figure 2 is included,[§] $n_{\text{light}} = 5$ is the number of light quarks, and $n_t = 1$ or 0 depending on whether or not the top quark is included in the effective theory. In this formula, we have written

$$b_0 = \frac{11}{3}C_A - \frac{4}{3}T_F(n_{\text{light}} + n_t) - \frac{1}{3}T_F \quad (2.15)$$

$$h(r) = \frac{2}{9}(4-r)\sqrt{1-r} - \frac{8}{9} - \frac{2}{3}\ln(1+\sqrt{1-r}) + \frac{2}{3}\ln(2) \quad (2.16)$$

$$r = m_t^2/m_{\tilde{t}_1}^2. \quad (2.17)$$

The function $h(r)$ is defined so that it parametrizes the effects of a non-zero top-quark mass. In

[§] In the MSSM, $\delta = 1$. However, one can imagine non-supersymmetric theories with fundamental strongly interacting scalars, in which these formulas would apply with $\delta = 0$.

the limit that the top quark is massless compared to the top squark we have $h(0) = 0$, and when the masses are identical we have $h(1) = -\frac{8}{9} + \frac{2}{3} \ln(2)$.

The one-loop order correction to the diphoton cross-section can now be found simply by dropping the diagrams that involve gluon self-coupling or real gluon emission (equivalent to setting $C_A = 0$) as well as any vacuum polarization diagrams (which no longer involve strong couplings), then making the replacement $\hat{g}_3 T_k^{aj} \rightarrow Q e \delta_k^j$ at vertices to change gluons into photons. Following this procedure, we find

$$v\sigma^{(1)}(\tilde{t}_1 \tilde{t}_1^* \rightarrow \gamma\gamma) = v\sigma^{(0)}(\tilde{t}_1 \tilde{t}_1^* \rightarrow \gamma\gamma) \left\{ 1 + f(\epsilon) \frac{\hat{\alpha}_S}{\pi} C_F \left[\frac{\pi^2}{v} - \frac{11}{2} + \frac{\pi^2}{8} - 2 \ln(2) \right] + \left(\frac{1}{2} - \frac{\pi^2}{8} \right) \delta \right\}. \quad (2.18)$$

In the $\overline{\text{MS}}$ renormalization scheme, the bare coupling $\hat{\alpha}_S$ is written in terms of the renormalized running coupling $\alpha_S(Q)$ using

$$\hat{\alpha}_S = \alpha_S \left[1 - \frac{\alpha_S}{4\pi} b_0 \left(\frac{1}{\epsilon_{\text{UV}}} + \ln(4\pi\mu^2/Q^2) - \gamma_E \right) \right]. \quad (2.19)$$

The gluon cross section as a function of the renormalized $\overline{\text{MS}}$ coupling α_S and the renormalization scale Q can therefore be written as

$$v\sigma^{(1)}(\tilde{t}_1 \tilde{t}_1^* \rightarrow gg) = v\sigma^{(0)}(\tilde{t}_1 \tilde{t}_1^* \rightarrow gg) \left\{ 1 + \frac{\alpha_S}{\pi} \left[\frac{b_0}{2} \ln\left(\frac{Q^2}{4m_{\tilde{t}_1}^2}\right) + \left(\frac{199}{18} - \frac{13\pi^2}{24}\right) C_A \right] + \left(\frac{\pi^2}{v} - \frac{7}{2} - \frac{\pi^2}{8} + \left(\frac{1}{2} - \frac{\pi^2}{8}\right) \delta\right) C_F \right. \\ \left. + \left(-\frac{16}{9}(n_{\text{light}} + n_t) - 2n_t h(m_{\tilde{t}}^2/m_{\tilde{t}_1}^2) - \frac{1}{3} \ln(2)\right) T_F \right\}. \quad (2.20)$$

For the diphoton final state, one can simply replace the bare coupling $\hat{\alpha}_S$ by the $\overline{\text{MS}}$ coupling α_S in eq. (2.18) to obtain the corresponding renormalized result for $v\sigma^{(1)}(\tilde{t}_1 \tilde{t}_1^* \rightarrow \gamma\gamma)$, since the QCD coupling does not appear in the tree-level result in that case.

The ratio of partial widths is now obtained at next-to-leading order by

$$R^{(1)} \equiv \frac{\Gamma^{(1)}(\eta_{\tilde{t}} \rightarrow \gamma\gamma)}{\Gamma^{(1)}(\eta_{\tilde{t}} \rightarrow \text{hadrons})}. \quad (2.21)$$

(Here we write “hadrons” to subsume the gg , ggg , and the partial $gq\bar{q}$ parton-level contributions.) The $1/v$ Coulomb singularity does not appear in this ratio, since it can be absorbed into a redefinition of the bound-state wavefunction factor [37], at least at order α_S in the approximation of a Coulombic bound state, and the redefined bound-state factor in turn cancels from the ratio of decay rates. This redefinition simply removes the $1/v$ part as it is expanded to next-to-leading order in α_S . There may remain some small residual dependence on $1/v$ proportional to α_S^2 , due to the fact that the bound-state potential is actually not exactly Coulombic, but this is beyond the

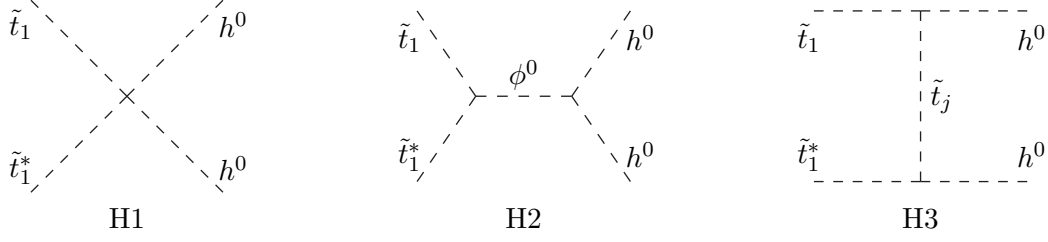


FIG. 5: The tree-level diagrams for the annihilation of $\tilde{t}_1\tilde{t}_1^*$ into h^0h^0 .

scope of the present work since we work only to order α_S in the ratio. Our final result is

$$\begin{aligned}
 R^{(1)} = & \frac{8\alpha^2}{9\alpha_S^2} \left\{ 1 + \frac{\alpha_S}{\pi} \left[-\frac{b_0}{2} \ln\left(\frac{Q^2}{4m_{\tilde{t}_1}^2}\right) + \left(\frac{13\pi^2}{24} - \frac{199}{18}\right) C_A + \left(\frac{\pi^2}{4} - 2 - 2\ln(2)\right) C_F \right. \right. \\
 & \left. \left. + \left(\frac{16}{9}(n_{\text{light}} + n_t) + 2n_t h(m_t^2/m_{\tilde{t}_1}^2) + \frac{1}{3}\ln(2)\right) T_F \right] \right\}. \quad (2.22)
 \end{aligned}$$

An interesting feature of this result is that the term proportional to C_A is the same for the stoponium and the corresponding quarkonium calculation as can be seen by comparing[¶] eq. (2.22) to eqs. (4.1)-(4.4) of ref. [30].

III. DECAYS TO HIGGS SCALAR BOSONS

We now consider the one-loop radiative corrections to $\eta_{\tilde{t}} \rightarrow h^0h^0$, where h^0 is the lightest Higgs scalar boson in supersymmetry. In this case we calculate the partial widths directly rather than using the cut method. The tree-level diagrams contributing to this annihilation decay are shown in figure 5. The corresponding annihilation cross-section in the $v \rightarrow 0$ limit can be written as [21] (see also [25, 29]):

$$v\sigma^{(0)}(\tilde{t}_1\tilde{t}_1^* \rightarrow h^0h^0) = \frac{N_c}{64\pi m_{\tilde{t}_1}^2} (1 - m_{h^0}^2/m_{\tilde{t}_1}^2)^{1/2} (\lambda_1 + \lambda_2 + \lambda_3)^2, \quad (3.1)$$

where, in the notation of ref. [35], the effective couplings are:

$$\lambda_1 = \lambda_{h^0h^0\tilde{t}_1\tilde{t}_1^*}, \quad (3.2)$$

$$\lambda_2 = \sum_{\phi^0=h^0, H^0} \lambda_{\phi^0\tilde{t}_1\tilde{t}_1^*} \lambda_{\phi^0h^0h^0} / (4m_{\tilde{t}_1}^2 - m_{\phi^0}^2), \quad (3.3)$$

$$\lambda_3 = \sum_{j=1,2} -2|\lambda_{h^0\tilde{t}_1\tilde{t}_j^*}|^2 / (m_{\tilde{t}_1}^2 + m_{\tilde{t}_j}^2 - m_{h^0}^2). \quad (3.4)$$

[¶] Note that $R^{(1)}$ in ref. [30] is the reciprocal of our definition.

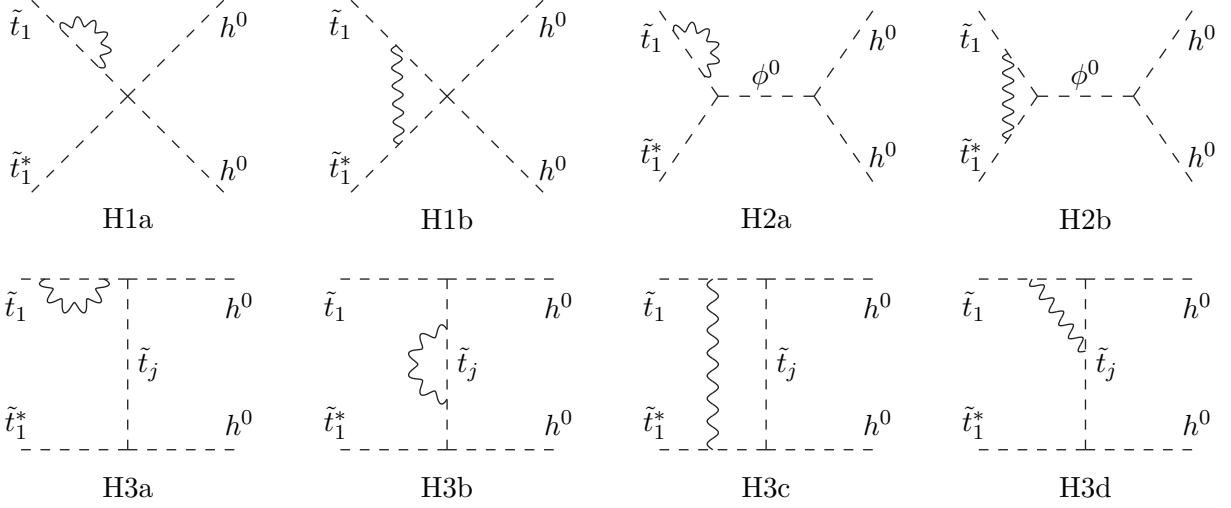


FIG. 6: The one-loop QCD diagrams for the annihilation of $\tilde{t}_1\tilde{t}_1^*$ into h^0h^0 .

diagram	C_{diagram}
H1a, H2a, H3a	$\frac{1}{2\epsilon_{\text{UV}}} - \frac{1}{2\epsilon_{\text{IR}}}$
H1b, H2b	$\frac{1}{2\epsilon_{\text{IR}}} + \frac{1}{4\epsilon_{\text{UV}}} + \frac{\pi^2}{2v} - \frac{1}{2} + \frac{3}{2}\ln(2)$
H3b	$\frac{1}{2\epsilon_{\text{UV}}} + 1 + \ln(2) + \frac{h}{2(1-h)}\ln(2-h)$
H3c	$\frac{1}{2\epsilon_{\text{IR}}} + \frac{\pi^2}{2v} - 1 - \ln(1-h/2) - \frac{h}{2-h}k_1(h) - \frac{1}{2}k_2(h)$
H3d	$\frac{1}{2\epsilon_{\text{UV}}} + 1 + \ln(2) - \frac{2-h}{2(1-h)}\ln(2-h) + \frac{1}{2}k_1(h) + k_2(h)$

TABLE III: Results for one-loop radiative corrections to $\tilde{t}_1\tilde{t}_1^* \rightarrow h^0h^0$, corresponding to the diagrams in figure 6 and appearing in eqs. (3.7), (3.8).

Using eq. 2.6), the tree-level ratio of $\gamma\gamma$ to h^0h^0 partial widths is therefore

$$\Gamma^{(0)}(\gamma\gamma)/\Gamma^{(0)}(h^0h^0) = \frac{2048\pi^2\alpha^2}{81(\lambda_1 + \lambda_2 + \lambda_3)^2}(1 - m_{h^0}^2/m_{\tilde{t}_1}^2)^{-1/2}. \quad (3.5)$$

The one-loop QCD corrections to the stoponium decay to h^0h^0 are due to the diagrams shown in figure 6. Note that there are no gluon emission diagrams to this process at this order, because the initial and final states are both color singlets. In this paper, we will neglect[†] in λ_3 the contribution of the heavier top-squark mass eigenstate \tilde{t}_2 , which would otherwise entail a somewhat more complicated kinematic loop integration. At one-loop order in QCD and in the limit of small v , the corresponding $\tilde{t}_1\tilde{t}_1^* \rightarrow h^0h^0$ result is:

$$v\sigma^{(1)}(\tilde{t}_1\tilde{t}_1^* \rightarrow h^0h^0) = \frac{N_c}{64\pi m_{\tilde{t}_1}^2}(1 - m_{h^0}^2/m_{\tilde{t}_1}^2)^{1/2} \left[C(\hat{\lambda}_1 + \hat{\lambda}_2) + C'\hat{\lambda}_3 \right]^2, \quad (3.6)$$

[†] The decay of stoponium to h^0h^0 is especially important in electroweak-scale baryogenesis models [11], [9], [12] that require light \tilde{t}_1 . In those models, $m_{\tilde{t}_2}$ is necessarily very large, making this approximation extremely good.

where, in terms of the individual diagram contributions given in Table III,

$$C = 1 + C_F \frac{\alpha_S}{\pi} f(\epsilon) (C_{H1a} + C_{H1b}), \quad (3.7)$$

$$C' = 1 + C_F \frac{\alpha_S}{\pi} f(\epsilon) (C_{H3a} + C_{H3b} + C_{H3c} + C_{H3d}). \quad (3.8)$$

The couplings $\widehat{\lambda}_{1,2,3}$ are given by the same formulas as eq. (3.2)-(3.4), but with bare couplings, denoted by $\widehat{\lambda}_{h^0 h^0 \tilde{t}_1 \tilde{t}_1^*}$, $\widehat{\lambda}_{\phi^0 \tilde{t}_1 \tilde{t}_1^*}$, and $\widehat{\lambda}_{\phi^0 h^0 h^0}$, in place of their unhatted counterparts. Also,

$$h \equiv m_{h^0}^2 / m_{\tilde{t}_1}^2, \quad (3.9)$$

and we have defined functions

$$k_1(h) = B \tan^{-1}(hB/(2-h)), \quad (3.10)$$

$$k_2(h) = \frac{2-h}{2A} \text{Re} \left[\text{Li}_2 \left(\frac{1+A}{1+iAB} \right) - \text{Li}_2 \left(\frac{1-A}{1+iAB} \right) \right] \\ + \frac{1}{2} \text{Li}_2 \left(1 - \frac{2A}{2-h} \right) - \frac{1}{2} \text{Li}_2 \left(1 + \frac{2A}{2-h} \right), \quad (3.11)$$

with $A = \sqrt{1-h}$ and $B = \sqrt{4/h-1}$, and $\text{Li}_2(x)$ is the dilogarithm function (also known as the Spence function). These functions have values $k_1(0) = 2$ and $k_2(0) = -\pi^2/8$ for the extreme limit $m_{h^0} \ll m_{\tilde{t}_1}$, and $k_1(1) = \pi/\sqrt{3}$ and $k_2(1) = -\pi/2\sqrt{3}$ near threshold for the decay. The calculation of these diagrams relies on loop integrals that can be found from refs. [33, 36] by taking the $v \rightarrow 0$ limit with appropriate special cases of momenta and masses. Note that the $1/\epsilon_{\text{IR}}$ poles cancel in eqs. (3.7) and (3.8), as required.

The bare couplings can be written in terms of the renormalized running $\overline{\text{MS}}$ scheme couplings $\lambda_{h^0 h^0 \tilde{t}_1 \tilde{t}_1^*}$, $\lambda_{\phi^0 \tilde{t}_1 \tilde{t}_1^*}$, and $\lambda_{\phi^0 h^0 h^0}$, at one-loop order in QCD, as:

$$\widehat{\lambda}_{h^0 h^0 \tilde{t}_1 \tilde{t}_1^*} = \lambda_{h^0 h^0 \tilde{t}_1 \tilde{t}_1^*} \left[1 - \frac{3\alpha_S}{4\pi} \left(\frac{1}{\epsilon_{\text{UV}}} + \ln(4\pi\mu^2/Q^2) - \gamma_E \right) \right], \quad (3.12)$$

$$\widehat{\lambda}_{\phi^0 \tilde{t}_1 \tilde{t}_1^*} = \lambda_{\phi^0 \tilde{t}_1 \tilde{t}_1^*} \left[1 - \frac{3\alpha_S}{4\pi} \left(\frac{1}{\epsilon_{\text{UV}}} + \ln(4\pi\mu^2/Q^2) - \gamma_E \right) \right], \quad (3.13)$$

$$\widehat{\lambda}_{\phi^0 h^0 h^0} = \lambda_{\phi^0 h^0 h^0}, \quad (3.14)$$

which eliminates the $1/\epsilon_{\text{UV}}$ dependence of the result up to terms of $\mathcal{O}(\alpha_S^2)$. It follows that

$$v\sigma^{(1)}(\tilde{t}_1 \tilde{t}_1^* \rightarrow h^0 h^0) = \frac{N_c}{64\pi m_{\tilde{t}_1}^2} (1 - m_{h^0}^2/m_{\tilde{t}_1}^2)^{1/2} K (\lambda_1 + \lambda_2 + K'\lambda_3)^2, \quad (3.15)$$

where $\lambda_{1,2,3}$ are as given in eqs. (3.2)-(3.4), with $\lambda_{h^0 h^0 \tilde{t}_1 \tilde{t}_1^*}$, $\lambda_{\phi^0 \tilde{t}_1 \tilde{t}_1^*}$, and $\lambda_{\phi^0 h^0 h^0}$ taken to be $\overline{\text{MS}}$ couplings, the masses renormalized on-shell, and

$$K = 1 + C_F \frac{\alpha_S}{\pi} \left[\frac{\pi^2}{v} + \frac{3}{2} \ln(Q^2/4m_{\tilde{t}_1}^2) - 1 + 3\ln(2) \right], \quad (3.16)$$

$$\begin{aligned}
K' = 1 + C_F \frac{\alpha_S}{\pi} & \left[\frac{3}{4} \ln(Q^2/4m_{\tilde{t}_1}^2) + \frac{3}{2} - \frac{1}{2} \ln(2) - 2 \ln(1 - h/2) \right. \\
& \left. + \left(\frac{1}{2} - \frac{h}{2-h} \right) k_1(h) + \frac{1}{2} k_2(h) \right]. \tag{3.17}
\end{aligned}$$

By comparing eqs. (2.18), (3.1), and (3.15), we obtain

$$\frac{\Gamma^{(1)}(\gamma\gamma)}{\Gamma^{(1)}(h^0 h^0)} = \frac{\Gamma^{(0)}(\gamma\gamma)}{\Gamma^{(0)}(h^0 h^0)} \frac{(\lambda_1 + \lambda_2 + \lambda_3)^2}{(\lambda_1 + \lambda_2 + K' \lambda_3)^2} \left(1 - C_F \frac{\alpha_S}{\pi} \left[\frac{3}{2} \ln(Q^2/4m_{\tilde{t}_1}^2) + 4 + 5 \ln(2) \right] \right), \tag{3.18}$$

written in terms of $\overline{\text{MS}}$ couplings and on-shell masses.

IV. NUMERICAL RESULTS

In this section, we will examine the numerical impact of the radiative corrections found above in typical realistic cases. In many models, the dominant final state is hadrons coming from the gg or ggg parton-level process at next-to-leading order in QCD. As found in ref. [29], this often amounts to 90% or more of the total decay width. (In particular, even when it is kinematically allowed, the $t\bar{t}$ final state is typically dominated by the gg final state and has a branching ratio of only a few per cent, unless there is a resonant Higgs exchange contribution.) Therefore, for simplicity we will begin by considering the idealized case that only diphoton and gluon-induced hadronic final states are included.

The relevant QCD group theory invariants for $SU(3)_c$ are $C_A = N_c = 3$, $C_F = (N_c^2 - 1)/2N_c = 4/3$, $T_F = 1/2$, and $n_{\text{light}} = 5$. At two-loop order, the QCD coupling runs according to [38]

$$Q \frac{d\alpha_S}{dQ} = -\frac{b_0}{2\pi} \alpha_S^2 - \frac{b_1}{4\pi^2} \alpha_S^3, \tag{4.1}$$

$$b_0 = \frac{23}{3} - \frac{2}{3} n_t - \frac{1}{6} n_s, \tag{4.2}$$

$$b_1 = \frac{58}{3} - \frac{19}{3} n_t - \frac{11}{6} n_s. \tag{4.3}$$

where n_t and n_s are either 0 or 1 depending on whether or not the top and stop, respectively, are included in the effective theory. Although we have not included the QED correction diagrams to the annihilation process, we do incorporate the running of the QED coupling according to

$$\alpha(Q) = \frac{\alpha(Q_0)}{1 + (b_0^{EM} \alpha(Q_0)/2\pi) \ln(Q/Q_0)}, \quad b_0^{EM} = -\frac{80}{9} - \frac{16}{9} n_t - \frac{4}{9} n_s. \tag{4.4}$$

We take as inputs $M_Z = 91.18$ GeV, $m_t = 172.5$ GeV, and $\alpha_S^{(5)}(M_Z) = 0.118$, $\alpha^{(5)}(M_Z) = 1/128.0$ as the running $\overline{\text{MS}}$ coupling inputs in the 5-quark Standard Model. We then determine $\overline{\text{MS}}$ couplings $\alpha_S(m_{\tilde{t}_1})$ and $\alpha(m_{\tilde{t}_1})$ by running below $Q = m_t$ using the 5-quark two-loop renormalization group equations, and, if $m_{\tilde{t}_1} > m_t$, running above $Q = m_t$ using the 6-quark renormalization group equations.

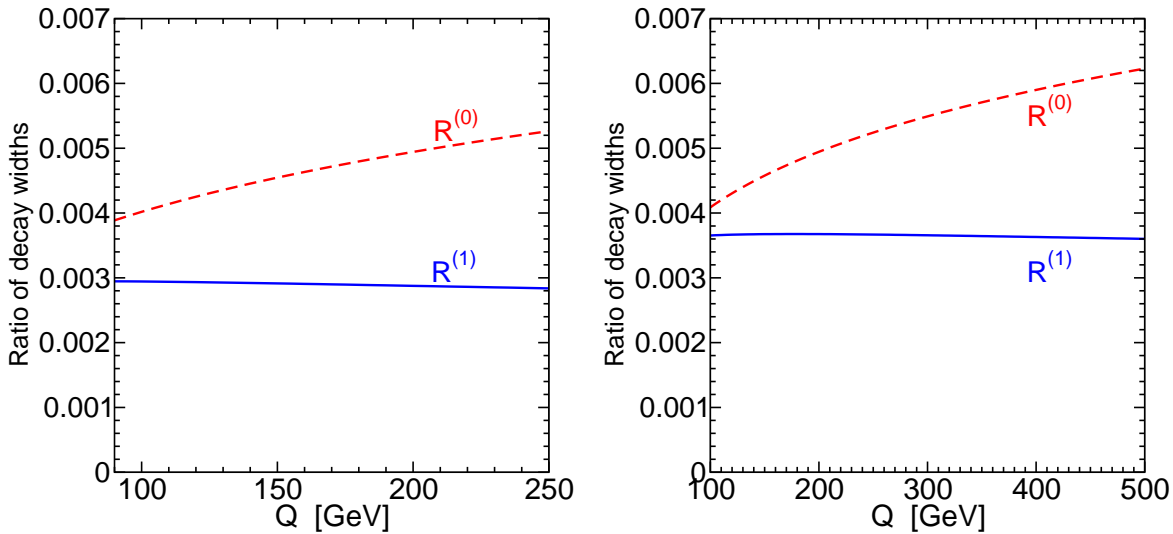


FIG. 7: The dependence of the ratio of decay widths of stoponium into $\gamma\gamma + X$ and into hadrons is shown at tree level ($R^{(0)}$, dashed lines) and at next-to-leading order in QCD, ($R^{(1)}$, solid lines), as a function of the $\overline{\text{MS}}$ renormalization scale Q . The left panel shows the results for $m_{\tilde{t}_1} = 120$ GeV and the right panel for $m_{\tilde{t}_1} = 225$ GeV, corresponding to approximately $m_{\eta_{\tilde{t}}} = 238$ GeV and 447 GeV, respectively.

Having determined the input parameter values at $Q = m_{\tilde{t}_1}$, we then match[†] onto and work in the effective theory in which the lighter top squark is always included (even for $Q < m_{\tilde{t}_1}$), so that $\alpha_S(Q)$ and $\alpha(Q)$ are obtained by running the renormalization group equations eq. (4.1) and (4.4) with $n_s = 1$ and either $n_t = 1$ (if $m_{\tilde{t}_1} > m_t$) or $n_t = 0$ (if $m_{\tilde{t}_1} < m_t$). We then evaluate the ratios of decay widths of stoponium into $\gamma\gamma + X$ and into hadrons at tree-level and at next-to-leading order, obtained from eqs. (2.7) and (2.22), respectively, self-consistently using the same value for n_t .

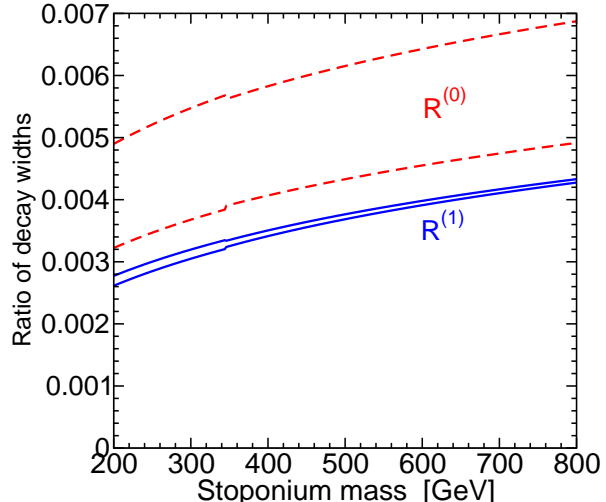
In figure 7, we compare the predicted ratios $R^{(0)}$ and $R^{(1)}$ as a function of the choice of $\overline{\text{MS}}$ renormalization scale Q , for two different choices of stop mass 120 and 225 GeV, corresponding to stoponium masses $m_{\eta_{\tilde{t}}} = 238$ and 447 GeV. The leading-order prediction has a strong scale dependence, which is not surprising since it is inversely proportional to α_S^2 . The next-to-leading order prediction for the branching ratio to photons is considerably smaller for all values of Q considered. For the choice $Q = m_{\tilde{t}_1}$, the decrease is roughly 30%. This may be considered somewhat unfortunate for the observability of the signal. We also note that the Q dependence of the predicted branching ratio is much improved by the next-to-leading order calculation.

Figure 8 shows the ratio of diphoton and hadronic decay widths as a function of the stoponium mass, computed at leading order and at next-to-leading order. The results are shown for two choices of the renormalization scale $Q = m_{\tilde{t}_1}/2$ and $Q = 2m_{\tilde{t}_1}$. Again we see that the diphoton branching ratio predicted by the next-to-leading order calculation is smaller than predicted at leading order.[‡] Taking into account the fact that the contributions of other final states ($h^0 h^0$, $W^+ W^-$, ZZ , and $t\bar{t}$) are quite model-dependent but can only decrease the diphoton branching ratio, we conclude

[†] We neglect threshold corrections when matching between different effective field theories, because they are of relative order α_S^2 and numerically small compared to other sources of error and uncertainty.

[‡] Small kinks are visible in the prediction curves in Figure 8 at $m_{\eta_{\tilde{t}}} = 2m_t$, due to our use of the 5-quark (6-quark) effective theory below (above) that threshold.

FIG. 8: The dependence of the ratio of decay widths of stoponium into $\gamma\gamma + X$ and into hadrons is shown at tree level ($R^{(0)}$, dashed lines) and at next-to-leading order in QCD, ($R^{(1)}$, solid lines), as a function of the stoponium mass $m_{\eta_{\tilde{t}}} \approx 2m_{\tilde{t}_1}$. The lower line in each case is the result for the renormalization scale choice $Q = m_{\tilde{t}_1}/2$, and the upper line is for $Q = 2m_{\tilde{t}_1}$.



that $\text{BR}(\gamma\gamma)$ is not more than about 0.25% for $m_{\eta_{\tilde{t}}} = 200$ GeV and 0.35% for $m_{\eta_{\tilde{t}}} = 500$ GeV.

It is somewhat more difficult to make a model-independent statement about the impact of the QCD radiative corrections for the $h^0 h^0$ final state. However, one can note that the factor K' appearing in eq. (3.15) is generally quite close to unity. Typical numerical values found from eq. (3.17) are $0.006 < K' - 1 < 0.021$ for $Q = m_{\tilde{t}_1}$ and $0.050 < K' - 1 < 0.065$ for $Q = 2m_{\tilde{t}_1}$. The lower range in each case occurs closer to threshold for the decay. Neglecting this small deviation from unity, one finds from eq. (3.18)

$$\left. \frac{\text{BR}(\gamma\gamma)}{\text{BR}(h^0 h^0)} \right|_{\text{NLO}} = \left. \frac{\text{BR}(\gamma\gamma)}{\text{BR}(h^0 h^0)} \right|_{\text{LO}} \left(1 - C_F \frac{\alpha_S}{\pi} \left[\frac{3}{2} \ln(Q^2/4m_{\tilde{t}_1}^2) + 4 + 5 \ln(2) \right] \right), \quad (4.5)$$

yielding a correction of order $(-23\%, -32\%)$ for $Q/m_{\tilde{t}_1} = (1, 2)$, respectively. This correction is comparable to, and has the same sign as, the ratio of the diphoton to the hadronic branching ratios. However, we note that the $\text{BR}(h^0 h^0)$ is itself highly model-dependent. It is generally quite small in the compressed supersymmetry models where top squarks mediate the annihilation of dark matter in the early universe, but can be very important in the models with light stops motivated by baryogenesis.

V. OUTLOOK

In this paper, we have calculated the stoponium decay rates to gg , $\gamma\gamma$ and $h^0 h^0$ at next-to-leading order in QCD, in order to obtain the branching ratio to two photons. Our calculation applies to the S -wave $J^{PC} = 0^{++}$ states, including the ground state that has the largest direct production cross-section. We have not included the $W^+ W^-$ and $Z^0 Z^0$ partial widths, which are often the next-largest contributions to the total stoponium decay rate, and have neglected the remaining decay channels, which have branching ratios of no more than a few percent at leading order.[†] However, it is worth noting that we can approximate the radiative corrections to the

[†] This includes the $t\bar{t}$ final state, which is dominated by the gg final state and so has a branching ratio of only a few percent even when $m_{\tilde{t}_1}$ is much larger than m_t , unless there is a resonance Higgs exchange contribution.

decay widths to W^+W^- and Z^0Z^0 , provided that the contributions from t-channel \tilde{b} and \tilde{t} squark exchange can be neglected. In this approximation, the radiative corrections come exclusively from 4-point and s-channel diagrams similar to H1a through H2b of figure 6, and it follows that the ratio of partial widths takes exactly the same form as eq. (4.5) with the Higgs branching ratio $\text{BR}(h^0h^0)$ replaced by $\text{BR}(W^+W^-)$ or $\text{BR}(Z^0Z^0)$ as appropriate.

This simplification applies to both of the model scenarios that motivate our study. In order to generate a relic density of dark matter in agreement with observation, models with compressed supersymmetry should have an LSP between about 170 and 270 GeV and a lightest stop mass eigenstate approximately 25 to 100 GeV heavier, which implies a stoponium mass very roughly between 400 and 700 GeV [4]. Within this range, there is extra suppression in the W^+W^- and Z^0Z^0 decay channels due to a cancellation between the terms of eq. (A.9) in ref. [29] that come from the 4-point and s-channel Higgs exchange diagrams (see also figure 5 of that paper for typical branching ratios as a function of stoponium mass in compressed supersymmetry). Even with a stoponium mass as high as 600 GeV, the combined W^+W^- and Z^0Z^0 decay rates represent no more than ten percent of the total width. In any case, the radiative corrections to the model-dependent terms arising from t-channel squark exchange are never large enough to make a big difference in the total $\text{BR}(\gamma\gamma)$.

In contrast, in models that feature electroweak-scale baryogenesis, the combined contribution to the stoponium decay rate from W^+W^- and Z^0Z^0 can be as large as about 50% at leading order (see figure 8 in ref. [29]). However, in this scenario W^+W^- and Z^0Z^0 decays from t-channel squark exchange are highly suppressed because the light stop consists almost entirely of the right-handed gauge eigenstate and the mass of the lightest sbottom is much greater than the mass of the lightest stop (for leading order amplitudes, see eqs. (A.5) through (A.10) of ref. [29]). Therefore the ratios of the $\gamma\gamma$ partial width to the W^+W^- and Z^0Z^0 partial widths will take the same form as eq. (4.5), with $\text{BR}(W^+W^-)$ or $\text{BR}(Z^0Z^0)$ in place of $\text{BR}(h^0h^0)$, to a very good approximation.

It should be noted [21] that the S -wave excited states of stoponium can be produced at the LHC with either direct decays to two photons or decays (with emission of soft mesons or photons) to lower stoponium states before annihilation. The treatment of direct annihilation decays of the excited S -wave states is the same as for the ground state. These contributions will be essentially indistinguishable in the $\gamma\gamma$ invariant mass signal, since the binding energy differences between such states will be less than the experimental resolution. However, part of the resulting signal will be lost when the excited S -wave states decay to P -wave states that decay directly [21]. Evaluating the contributions from excited states will require a more detailed understanding of the stoponium spectroscopy.

Although radiative corrections decrease the branching ratio significantly, stoponium annihilation to $\gamma\gamma$ is still a viable signal at the LHC. The approximately 30-35% reduction in the diphoton branching ratio found in this paper is likely to be offset by an enhancement due to radiative corrections to the cross-section for stoponium production in hadron colliders; note that the corresponding calculation for toponium production results in a K factor of roughly 1.3 or more [39]. We plan to report on the corresponding results for stoponium in a future paper. In any case, with sufficient integrated luminosity, stoponium should be visible, and the diphoton decay channel remains a unique opportunity for the direct and precise measurement of superpartner masses. Moreover, a measurement of the rate for $pp \rightarrow \eta_{\tilde{t}} \rightarrow \gamma\gamma$, taking into account the radiative corrections to both production and decay, will provide interesting and useful information about the stoponium system.

Acknowledgments: This work was supported in part by National Science Foundation grant PHY-0757325.

-
- [1] M. Drees, R. Godbole and P. Roy, “Theory and phenomenology of sparticles: An account of four-dimensional N=1 supersymmetry in high energy physics,” *World Scientific (2004)*; H. Baer and X. Tata, “Weak scale supersymmetry: From superfields to scattering events,” *Cambridge University Press (2006)*; S.P. Martin, “A supersymmetry primer,” [hep-ph/9709356] (version 5, December 2008). We use the notations of the last reference.
 - [2] The ATLAS collaboration, “ATLAS Detector and physics performance technical design report”, Volume 2. CERN-LHCC-99-15, ATLAS-TDR-15, May 1999.
 - [3] The CMS collaboration, “CMS Physics Technical Design Report”, Volume 1, Detector Performance and Software. CERN-LHCC-2006-001, CMS TDR 8.1, February 2006.
 - [4] S.P. Martin, Phys. Rev. D **75**, 115005 (2007) [hep-ph/0703097], Phys. Rev. D **76**, 095005 (2007) [hep-ph/0707.2812]. Phys. Rev. D **78**, 055019 (2008) [hep-ph/0807.2820].
 - [5] D.N. Spergel *et al.* [WMAP Collaboration], “Wilkinson Microwave Anisotropy Probe (WMAP) three year results: Implications for cosmology,” *Astrophys. J. Suppl.* **170**, 377 (2007) [astro-ph/0603449].
 - [6] M. Tegmark *et al.* [SDSS Collaboration], Phys. Rev. D **69**, 103501 (2004) [astro-ph/0310723].
 - [7] W.M. Yao *et al.* [Particle Data Group], “Review of particle physics,” *J. Phys. G* **33**, 1 (2006).
 - [8] M.E. Gomez, G. Lazarides and C. Pallis, Phys. Rev. D **61**, 123512 (2000) [hep-ph/9907261]; C. Boehm, A. Djouadi and M. Drees, Phys. Rev. D **62**, 035012 (2000) [hep-ph/9911496]; J.R. Ellis, K.A. Olive and Y. Santoso, *Astropart. Phys.* **18**, 395 (2003) [hep-ph/0112113].
 - [9] C. Balazs, M.S. Carena and C.E.M. Wagner, Phys. Rev. D **70**, 015007 (2004) [hep-ph/0403224]. C. Balazs, M.S. Carena, A. Menon, D.E. Morrissey and C.E.M. Wagner, Phys. Rev. D **71**, 075002 (2005) [hep-ph/0412264].
 - [10] G. Belanger, F. Boudjema, S. Kraml, A. Pukhov and A. Semenov, Phys. Rev. D **73**, 115007 (2006) [hep-ph/0604150].
 - [11] J.R. Espinosa, M. Quiros and F. Zwirner, Phys. Lett. B **307**, 106 (1993) [hep-ph/9303317], M.S. Carena, M. Quiros and C.E.M. Wagner, Phys. Lett. B **380**, 81 (1996) [hep-ph/9603420], Nucl. Phys. B **524**, 3 (1998) [hep-ph/9710401], J.R. Espinosa, Nucl. Phys. B **475**, 273 (1996) [hep-ph/9604320], D. Bodeker, P. John, M. Laine and M. G. Schmidt, Nucl. Phys. B **497**, 387 (1997) [hep-ph/9612364], M.S. Carena, M. Quiros, A. Riotto, I. Vilja and C.E.M. Wagner, Nucl. Phys. B **503**, 387 (1997) [hep-ph/9702409], J.M. Cline, M. Joyce and K. Kainulainen, Phys. Lett. B **417**, 79 (1998) [Erratum-ibid. B **448**, 321 (1999)] [hep-ph/9708393], JHEP **0007**, 018 (2000) [hep-ph/0006119], J.M. Cline and G.D. Moore, Phys. Rev. Lett. **81**, 3315 (1998) [hep-ph/9806354], M.S. Carena, M. Quiros, M. Seco and C.E.M. Wagner, Nucl. Phys. B **650**, 24 (2003) [hep-ph/0208043].
 - [12] M. Carena, G. Nardini, M. Quiros and C.E.M. Wagner, JHEP **0810**, 062 (2008) [hep-ph/0806.4297]. M. Carena, A. Freitas and C.E.M. Wagner, JHEP **0810**, 109 (2008) [hep-ph/0808.2298]. M. Carena, G. Nardini, M. Quiros and C.E.M. Wagner, “The Baryogenesis Window in the MSSM,” [hep-ph/0809.3760].
 - [13] J.L. Diaz-Cruz, J.R. Ellis, K.A. Olive and Y. Santoso, JHEP **0705**, 003 (2007) [hep-ph/0701229].
 - [14] K.-i. Hikasa and M. Kobayashi, Phys. Rev. D **36**, 724 (1987).
 - [15] C. Boehm, A. Djouadi and Y. Mambrini, Phys. Rev. D **61**, 095006 (2000) [hep-ph/9907428].
 - [16] M. Muhlleitner, A. Djouadi and Y. Mambrini, *Comput. Phys. Commun.* **168**, 46 (2005) [hep-ph/0311167].
 - [17] S.P. Das, A. Datta and M. Guchait, Phys. Rev. D **65**, 095006 (2002) [hep-ph/0112182].
 - [18] G. Hiller and Y. Nir, JHEP **0803**, 046 (2008) [hep-ph/0802.0916].
 - [19] K. Hagiwara, K. Kato, A.D. Martin and C.K. Ng, Nucl. Phys. B **344**, 1 (1990).
 - [20] M. Drees and M.M. Nojiri, Phys. Rev. Lett. **72**, 2324 (1994) [hep-ph/9310209].
 - [21] M. Drees and M.M. Nojiri, Phys. Rev. D **49**, 4595 (1994) [hep-ph/9312213].
 - [22] C.R. Nappi, Phys. Rev. D **25**, 84 (1982).

- [23] P. Moxhay and R.W. Robinett, Phys. Rev. D **32**, 300 (1985).
- [24] M.J. Herrero, A. Mendez and T.G. Rizzo, Phys. Lett. B **200**, 205 (1988).
- [25] V.D. Barger and W.Y. Keung, Phys. Lett. B **211**, 355 (1988).
- [26] H. Inazawa and T. Morii, Phys. Rev. Lett. **70**, 2992 (1993).
- [27] D.S. Gorbunov and V.A. Ilyin, JHEP **0011**, 011 (2000) [hep-ph/0004092].
- [28] N. Fabiano, Eur. Phys. J. C **19**, 547 (2001) [hep-ph/0103006].
- [29] S.P. Martin, Phys. Rev. D **77**, 075002 (2008) [hep-ph/0801.0237].
- [30] K. Hagiwara, C.B. Kim and T. Yoshino, Nucl. Phys. B **177**, 461 (1981).
- [31] R. Barbieri, E. d’Emilio, G. Curci and E. Remiddi, Nucl. Phys. B **154**, 535 (1979).
- [32] V.A. Novikov, L.B. Okun, M.A. Shifman, A.I. Vainshtein, M.B. Voloshin and V.I. Zakharov, Phys. Rept. **41**, 1 (1978).
- [33] W. Beenakker, H. Kuijf, W.L. van Neerven and J. Smith, Phys. Rev. D **40**, 54 (1989).
- [34] R.K. Ellis and G. Zanderighi, JHEP **0802**, 002 (2008) [hep-ph/0712.1851].
- [35] S.P. Martin, Phys. Rev. D **66**, 096001 (2002) [hep-ph/0206136], Phys. Rev. D **71**, 016012 (2005) [hep-ph/0405022].
- [36] G. ’t Hooft and M.J.G. Veltman, Nucl. Phys. B **153**, 365 (1979).
- [37] I. Harris and L.M. Brown, Phys. Rev. **105**, 1656 (1957). G.T. Bodwin, E. Braaten and G.P. Lepage, heavy Phys. Rev. D **51**, 1125 (1995) [Erratum-ibid. D **55**, 5853 (1997)] [hep-ph/9407339]. A. Petrelli, M. Cacciari, M. Greco, F. Maltoni and M.L. Mangano, Nucl. Phys. B **514**, 245 (1998) [hep-ph/9707223].
- [38] See, for example, M. Srednicki, “Quantum field theory,” *Cambridge, UK: Univ. Pr. (2007)*, eq. (78.36); D.R.T. Jones, Nucl. Phys. B **75**, 531 (1974).
- [39] J. H. Kuhn and E. Mirkes, Phys. Rev. D **48**, 179 (1993) [arXiv:hep-ph/9301204].